

# The synergistic effects of urbanization and an extreme heatwave event on urban thermal environment in Paris



Xiaojiao Ma <sup>a,b,c</sup>, Shiguang Miao <sup>a,c,\*</sup>, Valéry Masson <sup>d</sup>, Jean Wurtz <sup>d</sup>, Yizhou Zhang <sup>a,c</sup>, Jie Wang <sup>a,c</sup>, Xiang-Yu Huang <sup>a,c</sup>, Chao Yan <sup>a,c</sup>

<sup>a</sup> Institute of Urban Meteorology, China Meteorological Administration, Beijing, China

<sup>b</sup> Institute of Atmospheric Physics, Chinese Academy of Sciences, Beijing, China

<sup>c</sup> Key Laboratory of Urban Meteorology, China Meteorological Administration, Beijing, China

<sup>d</sup> CNRM, Université de Toulouse, Météo-France, CNRS, Toulouse, France

## ARTICLE INFO

### Keywords:

Heatwave  
Urban thermal environment  
Numerical simulation  
Hundred-meter-scale  
Surface energy budget

## ABSTRACT

In late July 2019, an extreme heatwave swept across the European regions. This study focused on examining the collective impacts of urbanization and this extreme heatwave on Paris's thermal environment. To achieve this, high-resolution simulations were performed using the urbanized version of the Weather Research and Forecasting (WRF) model. The inclusion of enhanced urban canopy parameters and improved spatial resolutions significantly improved the near-surface meteorological variables and the spatial-temporal patterns of the urban heat island in Paris. The impervious surface sensitivity study revealed that during the full-day sunlight conditions and low wind scenarios that characterized the extreme heatwave, the urban underlayer contributed to a 0.4 °C rise in daytime temperature and 1 °C increase during nighttime hours in the downtown area. Among the various representative Local Climate Zones (LCZ) types in Paris, namely compact mid-rise, large low-rise, and sparsely built, the contributions to temperature increase were about 0.3 °C (0.7 °C), 0.3 °C (0.5 °C), and 0.3 °C (0.6 °C) for daytime (nighttime) temperatures, respectively. The surface energy budget analysis further indicated that the augmented heat storage within urban impervious surfaces is one of the main causes of the enhanced urban heat island effect, particularly during the nighttime periods during heatwaves.

## 1. Introduction

Heatwaves are one of the most dangerous natural disasters and have severe negative impacts on organisms and ecosystems (Tan et al., 2007; Anderson and Bell, 2011). The last two decades in Europe have been characterized by numerous major heatwaves (Laaidi et al., 2012; Heaviside et al., 2016; Lhotka and Kyselý, 2022). Especially in these recent years, more frequent and more intense heatwaves have swept across the European region under the combined influence of large-scale circulation anomalies and human activities (Della-Marta et al., 2007; Stott et al., 2016; Rousi et al., 2022). As global warming continues to escalate and urbanization continues at a rapid pace worldwide, it is imperative to gain a comprehensive understanding of how urbanization affects the thermal environment in cities under different weather conditions. This knowledge is critical for effective urban planning and disaster management, with particular emphasis on addressing the challenges posed by extreme weather events.

\* Corresponding author at: Institute of Urban Meteorology, China Meteorological Administration, Beijing, China.  
E-mail address: [sgmiao@ium.cn](mailto:sgmiao@ium.cn) (S. Miao).

The inhomogeneous urban underlying surface, combined with anthropogenic heat and aerosol emissions, can affect the dynamic and thermal structure of the atmosphere and create the urban thermal environment represented by the urban heat island. Modeling and observational studies have demonstrated a synergistic effect between cities and heatwaves at different spatial and temporal scales (Li and Bou-Zeid, 2013; Li et al., 2015; Ramamurthy and Bou-Zeid, 2017; Ramamurthy et al., 2017; Zhao et al., 2018; Park et al., 2023). Ortiz et al. (2018) quantitatively studied the relative contributions of the urban underlying surface and weather conditions in New York City to the urban temperature and wind field during heatwaves, noting that the atmospheric circulation contributes mainly during the day, while the urban underlying surface plays a major role at night. Given the differences in climate background, city size, and land use among different cities, there are differences in the changes in urban heat island intensity and its interaction with heatwaves. Some studies suggest that the urban heat island effect is more significant during heatwaves (An et al., 2020; He et al., 2020), while other studies pointed out that under certain conditions, such as smaller cities (Ramamurthy and Bou-Zeid, 2017) or certain circulation situations (An et al., 2020; Ha et al., 2022), the urban heat island intensity may not increase during heatwaves or may even decrease (Richard et al., 2021).

Accurate weather forecasting depends on the development of high-resolution models. Meteo France organized the “Olympic Games 2024” research demonstration project that focuses on the Paris 2024 Olympic Games and to advance research on “future 100m (or finer) resolution meteorological forecasting systems for urban areas”. A series of studies have shown that compared with kilometer-resolution models, hundred-meter-resolution models can better represent surface features (Boutle et al., 2016) and explicitly solve some physical processes to replace traditional parameterization schemes. In terms of the urban modeling, many researchers have developed and improved urban land surface models in the past decade (Salamanca et al., 2010; Miao and Chen, 2014; Yang et al., 2015; Li et al., 2017) to better represent cities, providing powerful tools to study the influence of urban morphology and spatial structure on local or regional weather and climate, i.e., urban heat island (Miao et al., 2009; Ronda et al., 2017; Hollósi et al., 2021; Ma et al., 2023).

During late July 2019, Western Europe experienced a widespread extreme heatwave that broke high temperature records in most European countries, making it the strongest heatwave event in the region in recent years (Lhotka and Kysely, 2022). The highest temperature in Paris reached 42.6 °C on the afternoon of July 25, breaking the historical record set in July 1947. Given that Paris is one of the most densely populated cities in the world, landlocked, flat and almost free of the effects of large terrain, the urban heat island is thought to be more pronounced than in most cities (Oke et al., 2017). This paper aims to use a 111 m-resolution model to study the meteorological characteristics during the extreme heatwave event in Western Europe in July 2019 and to explore the synergies between the heatwave process and the urban environment in Paris, i.e., the influence of the urban thermal and dynamic environment during the different phases of the extreme heatwave. Moreover, surface energy budget analysis was conducted to elucidate the synergistic influence mechanisms of the urbanization and the heatwave on the thermal environment.

## 2. Data and method

This section describes the model and experimental setup, as well as the data used, including situ observations, reanalysis data, and static remote sensing data used in the simulation.

### 2.1. Observations and reanalysis data

To illustrate the spatiotemporal variations of the heatwave and to evaluate the performance of the model simulation, hourly data of nine reference meteorological stations distributed throughout the Greater Paris region during July 20–30 were applied. Elements included are near-surface air temperature, relative humidity, 10 m wind speed, 10-m wind direction, global radiation flux, precipitation, et al. The hourly fifth generation atmospheric reanalysis (ERA5) dataset from the European Center for Medium-Range Weather Forecasts (ECMWF) was used for model initial and boundary conditions as well as for heatwave weather analysis, with a spatial resolution of  $0.1^\circ \times 0.1^\circ$  for land surface and  $0.25^\circ \times 0.25^\circ$  for pressure levels, covering the period from 20th to 30th July 2019.

**Table 1**  
Basic settings for the model.

	D1	D2	D3	D4
Resolution (km)	9	1	0.333	0.111
Time step (s)	54	6	2	0.4
Vertical Level	82	105	105	105
Cumulus physics	Kain-Fritsch	0		
PBL physics	Boulac		Zhou et al., 2021	
Microphysics	Thompson scheme			
Longwave radiation	RRTMG scheme			
Shortwave radiation	RRTMG scheme			
Land-surface physics	Noah-MP land-surface model			
Urban physics	BEP			
Surface-layer physics	Revised MM5 Monin-Obukhov scheme			

## 2.2. Model configuration

The Rapid-refresh Multi-scale Analysis & Prediction System (RMAPS)\_Urban model developed by the Institute of Urban Meteorology, CMA, Beijing (Zhang et al., 2013) was used to simulate the persistent heatwave in Western Europe in late July 2019. The model uses Weather Research and Forecasting (WRF) version 4.3.3 and the coupled Noah\_MP land surface model and the BEP multi-layer urban canopy scheme. Table 1 presents the basic model settings. The nested domains were constructed with horizontal grid spacings of 9 km, 1 km, 333 m, and 111 m, centered on the Louvre Museum ( $48^{\circ}51'39.02''N$ ,  $2^{\circ}20'12.04'E$ ). The grid point dimensions were  $463 \times 463$ ,  $496 \times 496$ ,  $496 \times 496$ , and  $601 \times 601$ , respectively.

Vertical grid nesting (VN) was used to reduce numerical errors due to large aspect ratios on coarse grids while allowing for higher vertical resolution on fine grids. Specifically, the 9 km resolution model has 82 vertical layers in the first domain, with 29 layers below 1 km and the lowest level set at approximately 32 m above ground surface. While the second to fourth domains have 105 vertical layers, with 30 layers below 1 km and a minimum height of 15 m. For the physical options, the Thompson microphysics scheme, the RRTMG longwave radiation scheme, the RRTMG shortwave radiation scheme, and the Revised MM5 Monin-Obukhov surface layer scheme were selected. The Kain-Fritsch cumulus cloud scheme and the Boulac boundary layer scheme were used in the first domain, while the cumulus cloud scheme was turned off and a three dimension grid-aware PBL scheme was applied in other domains (Zhou et al., 2021).

Fig. 1 shows the nested domains and topographic elevations of the model. The outermost domain (D01) covers most of Europe and North Africa, while the innermost domain (D04) covers most of the Paris metropolitan area, including the central district of Paris. Paris is located on both sides of the Seine River in the center of the Paris Basin, with relatively flat topography. For the innermost domain, the NASA Shuttle Radar Topographic Mission (SRTM) 90 m DEM digital elevation database was used to provide high-resolution geographic information. Compared to the 9 km and 1 km grids, the 333 m and 111 m sub-kilometer grids are more accurate in representing the terrain and can better reflect small-scale terrain undulations. Among the nine sites shown in Fig. 1b, the deviation range of 111 m resolution is  $-2.5 \text{ m} \sim 1.3 \text{ m}$ , and the deviation range of 9 km resolution is  $-61 \text{ m} \sim 26 \text{ m}$ .

## 2.3. Gridded urban canopy parameter datasets

High-resolution (100 m) gridded urban canopy parameters (UCPs), including the gridded Open Street Map (OSM) urban fraction (UFRAC) dataset computed using the Geoclimate tool (Bocher et al., 2021) as well as the 100-m-resolution MApUCE land use/land

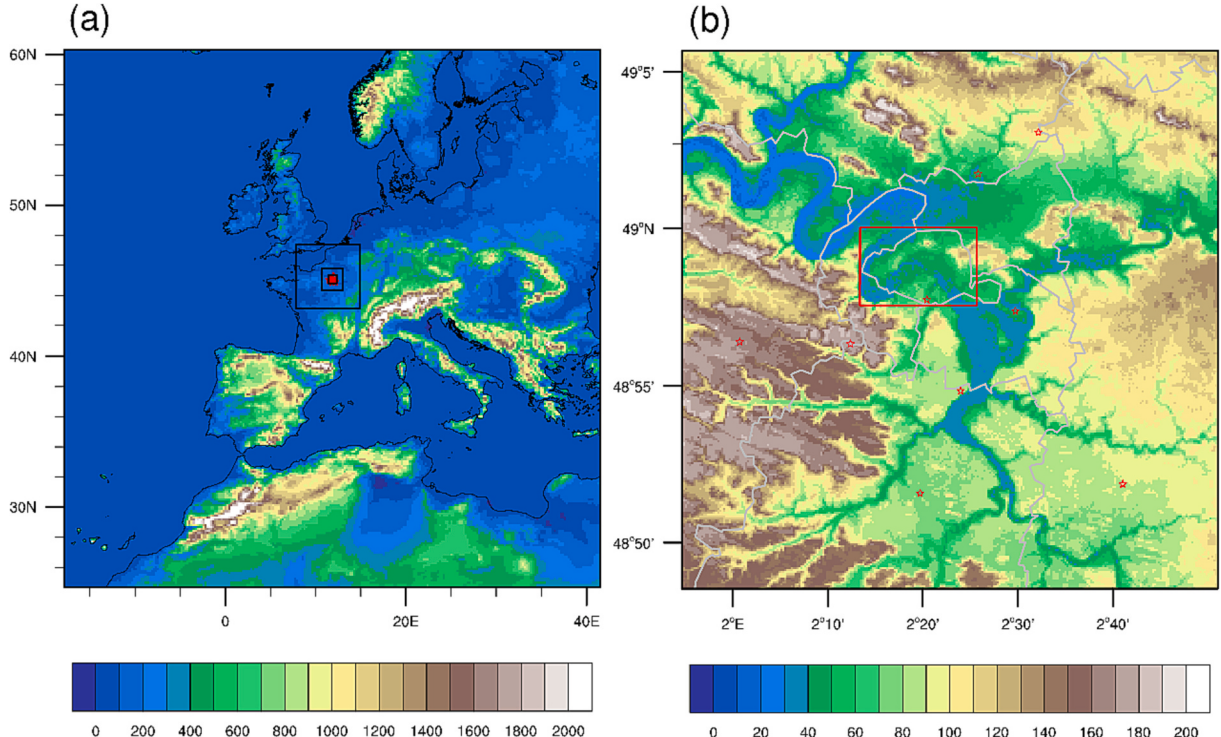


**Fig. 1.** Nested settings for the model. The shaded colour represents the terrain height (m). The outermost frame represents the d01 area, and the inner areas are d02, d03, and d04. The red pentagram indicates the location of the reference meteorological station, the red frame in Fig. 1b illustrates the central built-up areas of Paris. (For interpretation of the references to colour in this figure legend, the reader is referred to the web version of this article.)

cover (LULC) data (Bocher et al., 2018), and in which the urban was represented by the gridded Local Climate Zone (LCZ, Oke et al., 2017) map of Paris. Fig. 2 shows the distribution of LULC in the Paris metropolitan area. The statistical results further show that the compact buildings (LCZ2–3) take up a proportion of about 38%, which are mainly distributed in the core area of Paris, while large low-rise (LCZ8) and sparsely built (LCZ9) dominated the suburbs, accounting for 25.5% and 27.8% respectively.

#### 2.4. Numerical experimental design

The model uses ERA5 reanalysis data as initial and boundary conditions, and simulated three time periods from July 20–21, 22–23, and 24–25, 2019, each episode is initiated at 00 UTC, with the integration time of 48 h.

Four sets of sensitivity tests were designed to explore the enhancement effect of the addition of high-resolution static data and model setting on the simulation of near-surface meteorological elements, namely CTL, UFRAC, LCZ, and UFRAC+LCZ + VN tests. In addition, to study the influence of urban surface and physical processes on local meteorological conditions, this study conducted a comparative analysis of underlying surface sensitivity through control experiments with urban underlying surfaces (URB) and sensitivity experiments replacing the original urban underlayer with the croplands (NO.URB). See Table 2 for details.

### 3. Results

#### 3.1. Heatwave process in July 22–25th 2019

In the final days of July 2019, an extreme heat wave swept across Western Europe, breaking previous temperature records in numerous countries. Paris experienced an unprecedented high temperature of 42.6 °C, surpassing the previous record set in July 1947. Fig. 3 illustrates the daily variations of meteorological elements observed at two sites: the urban Montsouris site in Paris and the rural Melun site, covering the period from July 20–29, 2019. The Montsouris site, located in Montsouris Park and surrounded by mid-rise buildings, contrasts with the Melun site, located on the southeastern outskirts of Paris in an area dominated by cropland. Prior to the onset of the heat wave, Paris was shrouded in clouds, with some stations reporting night-time precipitation. The maximum temperature on July 20–21 remained below 30 °C. However, from July 22, temperatures in Paris rose steadily. On the afternoon of July 25, the Montsouris Park station recorded the highest temperature of the period, reaching 41.7 °C.

Throughout the heatwave, both urban and rural temperatures increased, but there were notable differences between the two locations. Throughout the day, the temperature variation between urban and rural areas remains slight, while the contrast in relative humidity is significant. It is worth highlighting that on the night of July 25, the specific humidity in Paris reached its lowest level, whereas it remained higher throughout the entirety of July 24. These observations align with the findings presented by An et al.

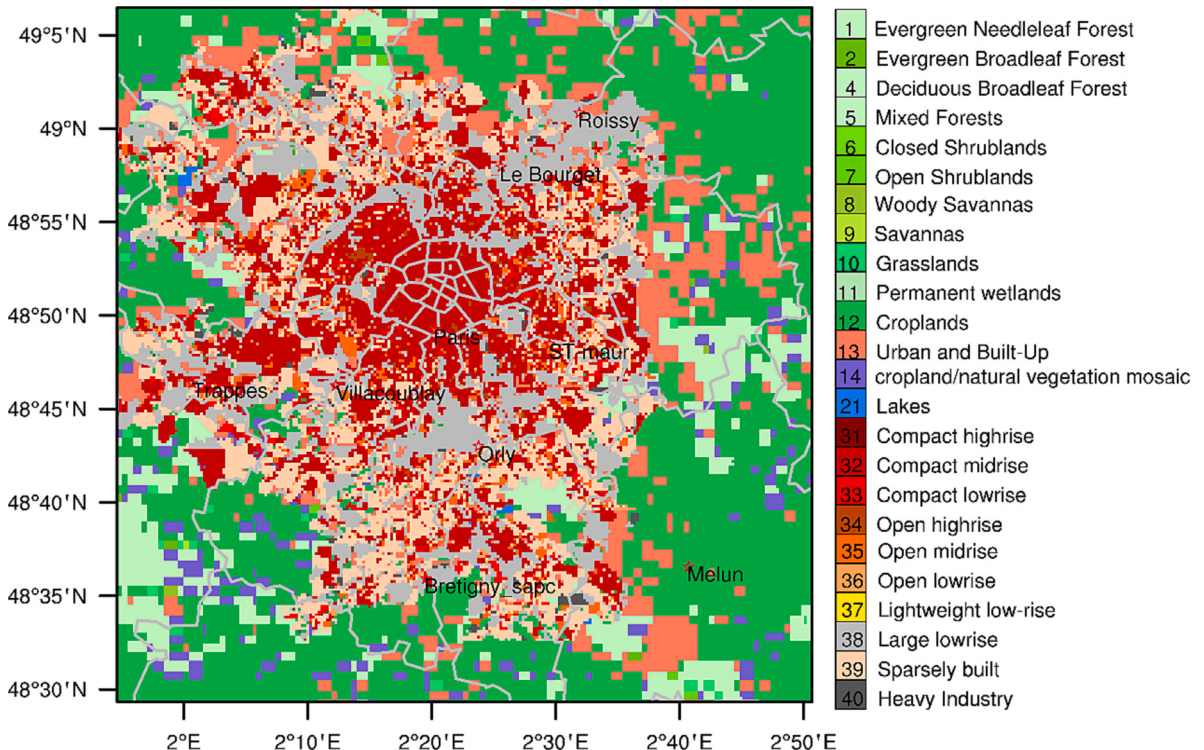
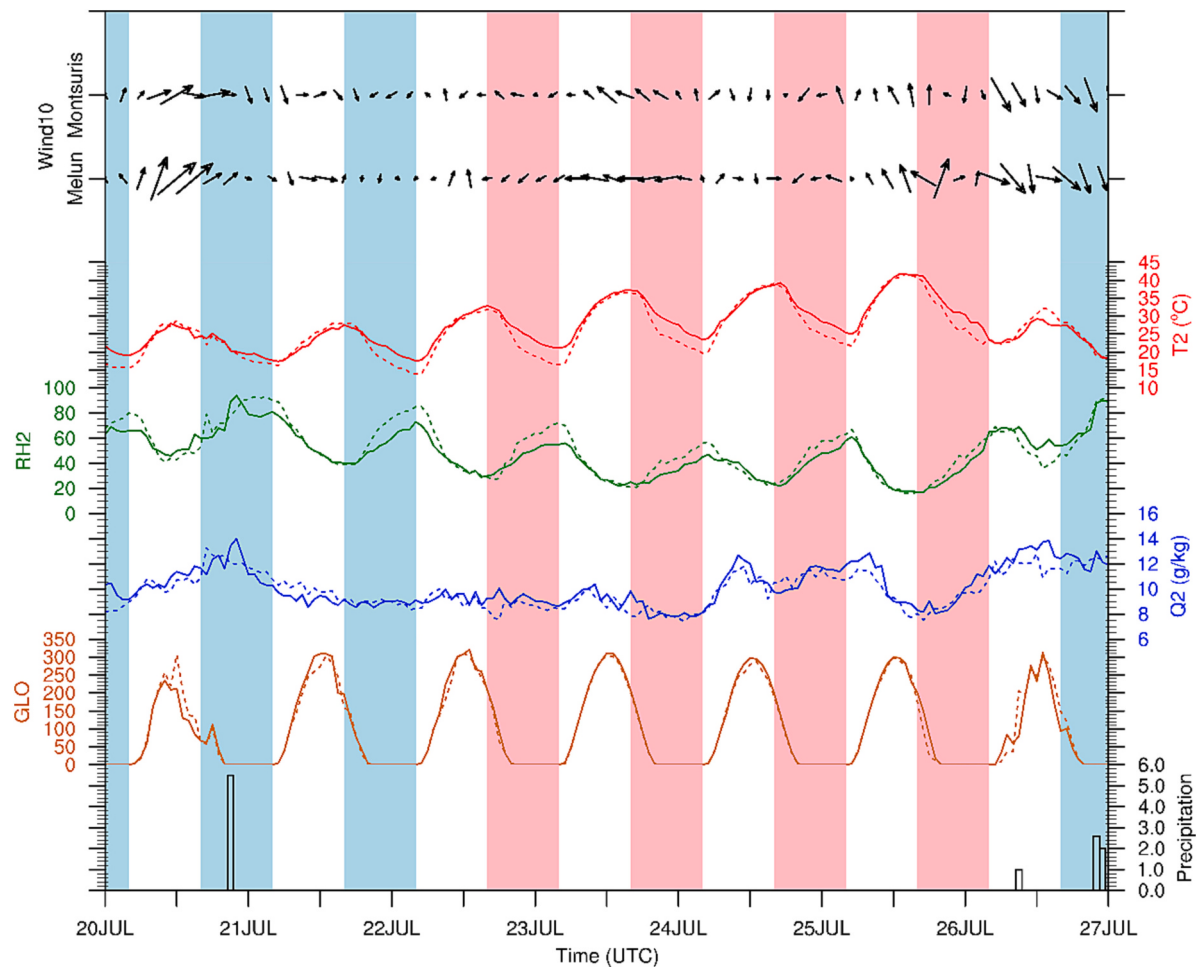


Fig. 2. Land use/land cover in the Paris metropolitan area.

**Table 2**  
Sensitive tests definition and setup.

Tests	Gridded urban fraction data	LULC	Vertical levels (D01-D04)	Urban scheme
CTL	FALSE	MODIS	59, 59, 59, 59	BEP
UFRAC	TRUE	MODIS	59, 59, 59, 59	BEP
LCZ	FALSE	LCZ	59, 59, 59, 59	BEP
UFRAC+LCZ + VN	TRUE	LCZ	82, 105, 105, 105	BEP
URB	TRUE	LCZ	82, 105, 105, 105	BEP
NO_URB	FALSE	Urban - > Croplands	82, 105, 105, 105	0



**Fig. 3.** Temporal variations of meteorological elements at the Montsouris and Melun stations in Paris from the 20th to the 29th: from top to bottom, there are 10-m wind vector, 2-m air temperature (red line), 2-m relative humidity (green line), 2-m specific humidity (blue line), global radiation (orange line), and precipitation (bar chart), respectively. (For interpretation of the references to colour in this figure legend, the reader is referred to the web version of this article.)

(2020). Further results indicate that the enhanced advection transport on July 25 resulted in a reduction of atmospheric water vapor content. While the combination of elevated temperatures and gentle surface winds on 24 July led to an intensified evaporation, subsequently increasing the overall water vapor content in the region (figure not shown).

Previous research has indicated that certain unusual atmospheric patterns, such as double jets and associated atmospheric blocking, may have a significant influence on the occurrence of heatwaves in Europe over a long-term climatological period (Black et al., 2004; Stefanon et al., 2012; Rousi et al., 2022; He et al., 2023). This study employs ERA5 reanalysis data to investigate the specific weather mechanisms behind a heatwave. The circulation patterns on the afternoons of the 22nd and 25th are illustrated in Figs. 4 and 5, respectively, while Fig. 6 displays the variations in vertical velocity and temperature advection at the Montsouris station, as calculated from the reanalysis data.

Between the 21st-23rd, a ridge of high pressure gradually formed in the middle and lower atmosphere, stretching northward across

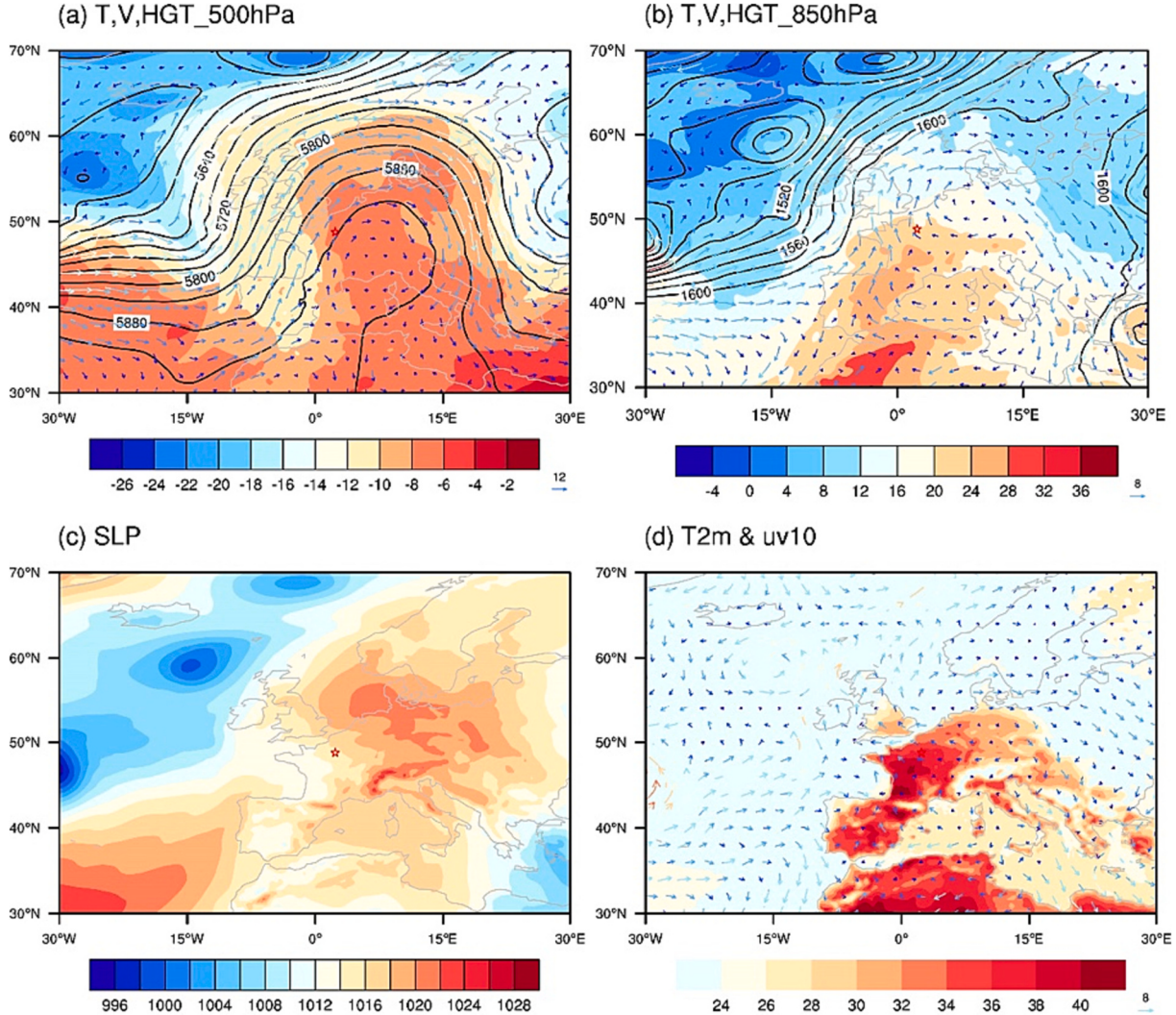


**Fig. 4.** Circulation fields on 22 July at 14UTC: (a) 500 hPa height field (shaded, unit: gpm), temperature field (contour, unit: °C), and wind vector; (b) 850 hPa height field (shaded), temperature field (contour), and wind vector; (c) sea level pressure field, unit: hPa; (d) 2-m temperature field (shaded, unit: °C) and 10-m wind vector.

central Europe. Paris was located near this high-pressure ridge (Fig. 4a), resulting in the accumulation of warm air in the lower troposphere (Fig. 4b). Combining the effects of subsidence heating (Fig. 6a) and radiation heating, the temperature in Paris experienced a gradual increase (Fig. 3). On the 24th, Paris remained under the influence of the ridge (figure not shown), with weak westerly surface winds and temperatures similar to those on the 23rd. By the 25th, a cyclone had formed and moved eastward towards France (Fig. 4), leading to an intensification of the low-level southerly winds (Fig. 3). This resulted in the noticeable transport of warm air masses from North Africa through warm advection (Fig. 5b), combined with clear-sky radiation heating, and caused a rapid temperature surge in Paris. On the 26th, cold air gradually infiltrated behind the trough, bringing light precipitation to Paris (Fig. 3). Subsequently, the heatwave event came to an end.

To summarize, at the beginning of the heat wave, a stable ridge of high pressure formed over Paris, accompanied by a weak downward motion in the middle and lower atmospheric layers. This resulted in mostly sunny conditions with minimal cloud cover and limited convection over most of Europe. The combination of strong clear sky radiation and low soil moisture contributed to an increase in the sensible heat flux. As the heatwave progressed, there was a significant transport of warm air from North Africa (warm advection). These dynamical and thermal conditions synergistically led to a sustained increase in temperature in Paris. A detailed examination of the influence of cities on urban thermal environment is presented in part 3.3.

### 3.2. Validation of the model during the heatwave event

In response to the extreme heat wave event in Paris in late July 2019, we performed high-resolution simulations of weather

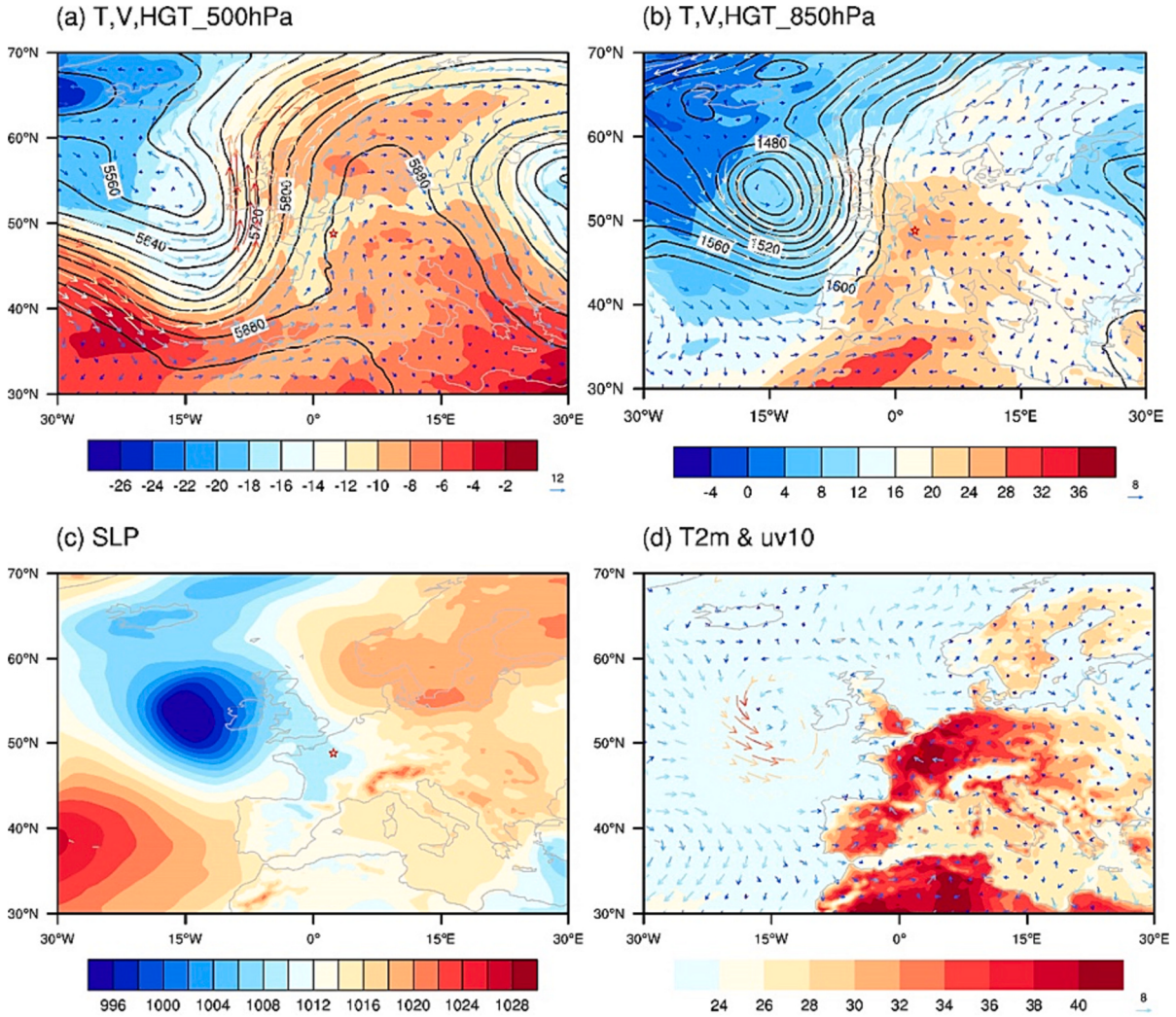


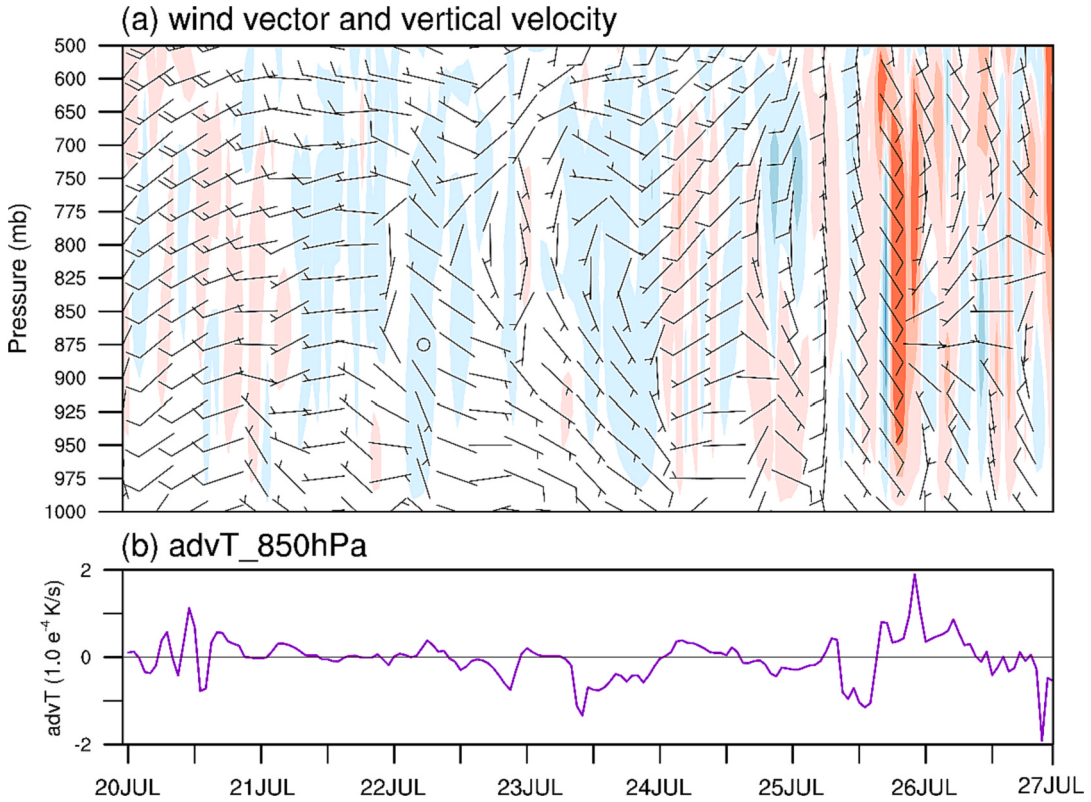
**Fig. 5.** Same as Fig. 4, but for circulation fields on July 25 at 14UTC.

processes during July 22–25. The simulated atmospheric and surface circulation patterns are in good agreement with the reanalysis results and the observations (figure omitted). It is worth noting that the addition of high-resolution static data, such as the LCZ and the impervious urban fraction (UFRAC), greatly improved the simulation of near-surface meteorological variables, especially the nighttime temperature and wind fields, and the addition of these data improved the 2-m temperature forecast of most urban stations by between 18% and 43% (Fig. 7).

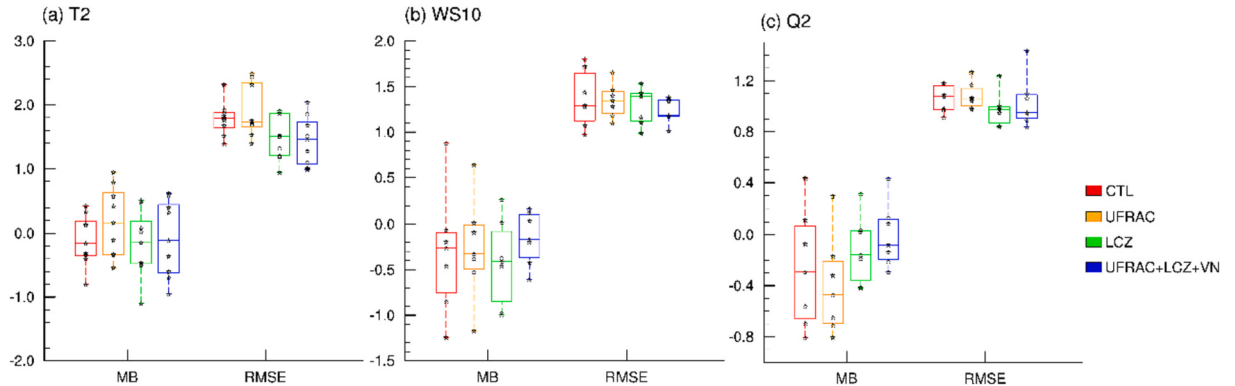
The evaluation of the performance of the kilometer and hundred-meter resolution models was performed using the Taylor diagram method (Taylor, 2001) (Fig. 8). As the grid resolution increased, the simulation results showed improved correlation and reduced overall deviations compared to the observations. Among the model grids, the 111-m resolution model showed superior performance in simulating humidity and wind speed, especially in urban areas where it closely matched the observations. This can be attributed to the more comprehensive consideration of energy balance in the multi-layer urban canopy scheme. A drawback of the simulation was an overestimation of the nighttime temperature, with a slight underestimation of the wind speed, especially during the night of the 24th.

Fig. 9 displays the changes in the 2-m temperature at the Montsouris and Melun stations, along with the Urban Heat Island Index (UHII) calculated as the temperature difference between these two stations. Fig. 10 depicts the spatial distribution of near surface features for both 111 m model and observations at 06:00 and 16:00 local time on 24 and 25 July. Overall, the 111-m resolution model shows accurate simulations of wind direction and speed despite some minor positional deviations, and reproduces the daily temperature fluctuations accurately, although it slightly overestimates the overnight lows on July 21 and 22.

Figs. 9 and 10 both show the presence of the urban heat island effect in Paris characterized by larger temperature differences between the city center and the suburbs at night than during the day, whereas the UHII exhibits significantly higher values at night compared to daytime. In addition, the UHII's temporal variation reveals minimal changes during the daytime throughout the heatwave period, whereas a notable increase in the heat island effect occurs at night. Starting from the early evening of the 21st, the temperature



**Fig. 6.** Temporal variations of meteorological elements at the Montsouris station in Paris from the 20th to the 26th: (a) horizontal wind vectors and vertical velocity field (shaded region, blue represents downdrafts, red represents updrafts); (b) 850 hPa temperature advection. Wind speed is in units of  $\text{m}\cdot\text{s}^{-1}$ , and temperature advection is in units of  $1.0\text{e}^{-4} \text{ K}\cdot\text{s}^{-1}$ . Calculated and plotted from ERA5 reanalysis data. (For interpretation of the references to colour in this figure legend, the reader is referred to the web version of this article.)



**Fig. 7.** Box line plots of the (a) 2-m air temperature, (b) 10-m wind speed, and (c) 2-m specific humidity difference between CTL, UFRAC, LCZ and UFRAC+LCZ + VN experiments. In the box, the horizontal line is the median, the ends of vertical lines are maximum and minimum values, and the markers represent statistical values for the nine stations. MB is mean bias from the observations, and RMSE is the root mean square error.

disparity between the city center and its outskirts escalates, indicating a prominent nocturnal heat island, which reaches its peak on the nights of the 22nd and 23rd. On the 24th, the daytime heat island effect weakens, and there are instances where Melun experiences higher temperatures than the city center. Overall, the model successfully captures the daily fluctuations in the heat island effect and accurately simulates the intensity of maximum and minimum temperatures, making it well-suited for studying the urban heat island phenomenon.

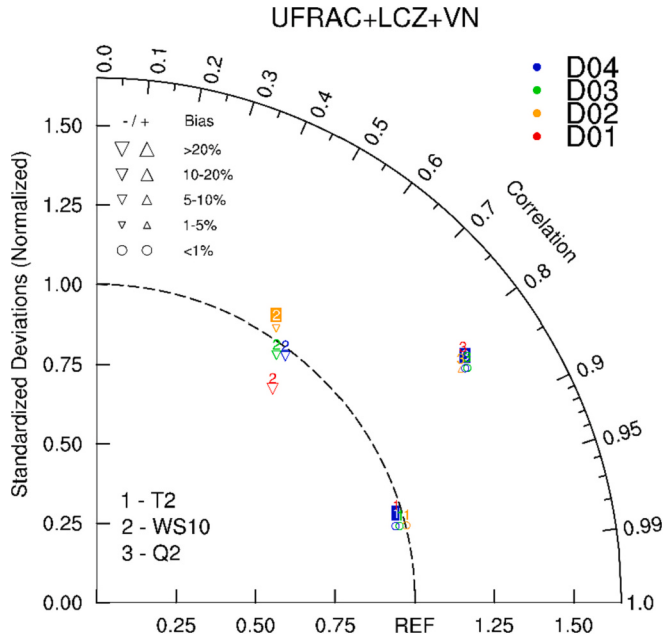


**Fig. 8.** Taylor diagrams of numerical simulation results for different regions. Numbers 1 to 3 represent 2-m air temperature, 10-m wind speed, and 2-m specific humidity, respectively. Regions D01 to D04 are represented by the colors red, orange, green and blue, respectively. The diagrams below the numbers indicate the percentage deviation of the simulated values from the observed values, and the shaded variables indicate the experiment with a smallest percentage deviation. (For interpretation of the references to colour in this figure legend, the reader is referred to the web version of this article.)

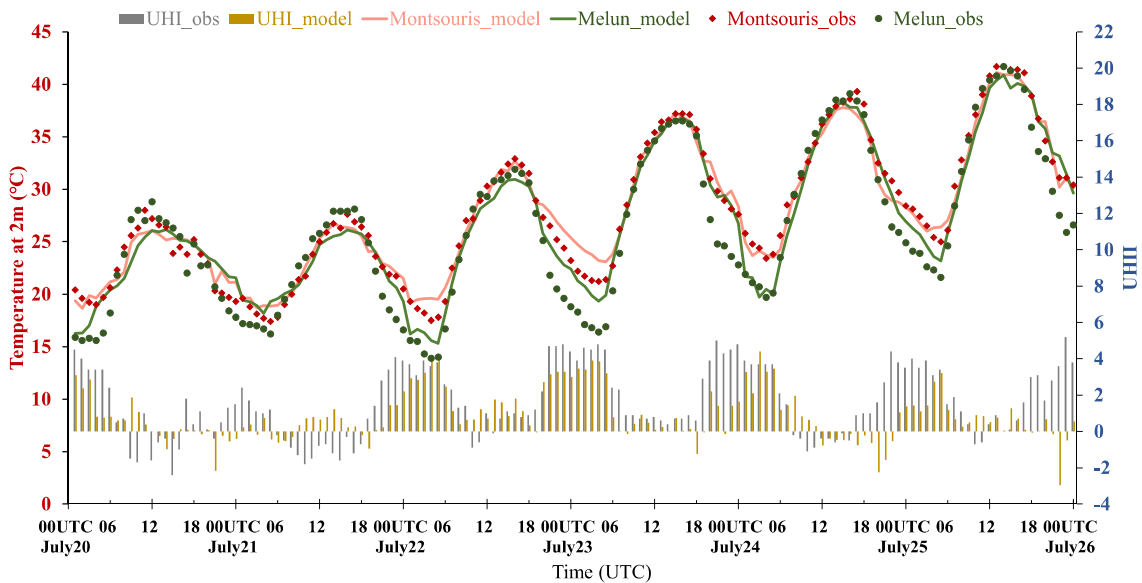


**Fig. 9.** Observed and 111-m model simulated 2-m temperature and urban heat island intensity index (UHII) ( $^{\circ}\text{C}$ ) variation curves for July 20–25 at the Montsouris and Melun stations, where the dotted lines are the observed values and the solid lines are the 111-m simulated values, red for the Montsouris station and green for the Melun station. The yellow and gray bars represent the simulated and observed UHII values, respectively. (For interpretation of the references to colour in this figure legend, the reader is referred to the web version of this article.)

### 3.3. Synergies between the extreme heatwave event and the urbanization

The urban thermal environment has a significant impact on the local climate, a sensitivity experiment is set up by changing the urban underlayer (URB) to cropland (NO.URB). Fig. 11 shows the anomaly distribution of temperature, humidity, and wind fields in

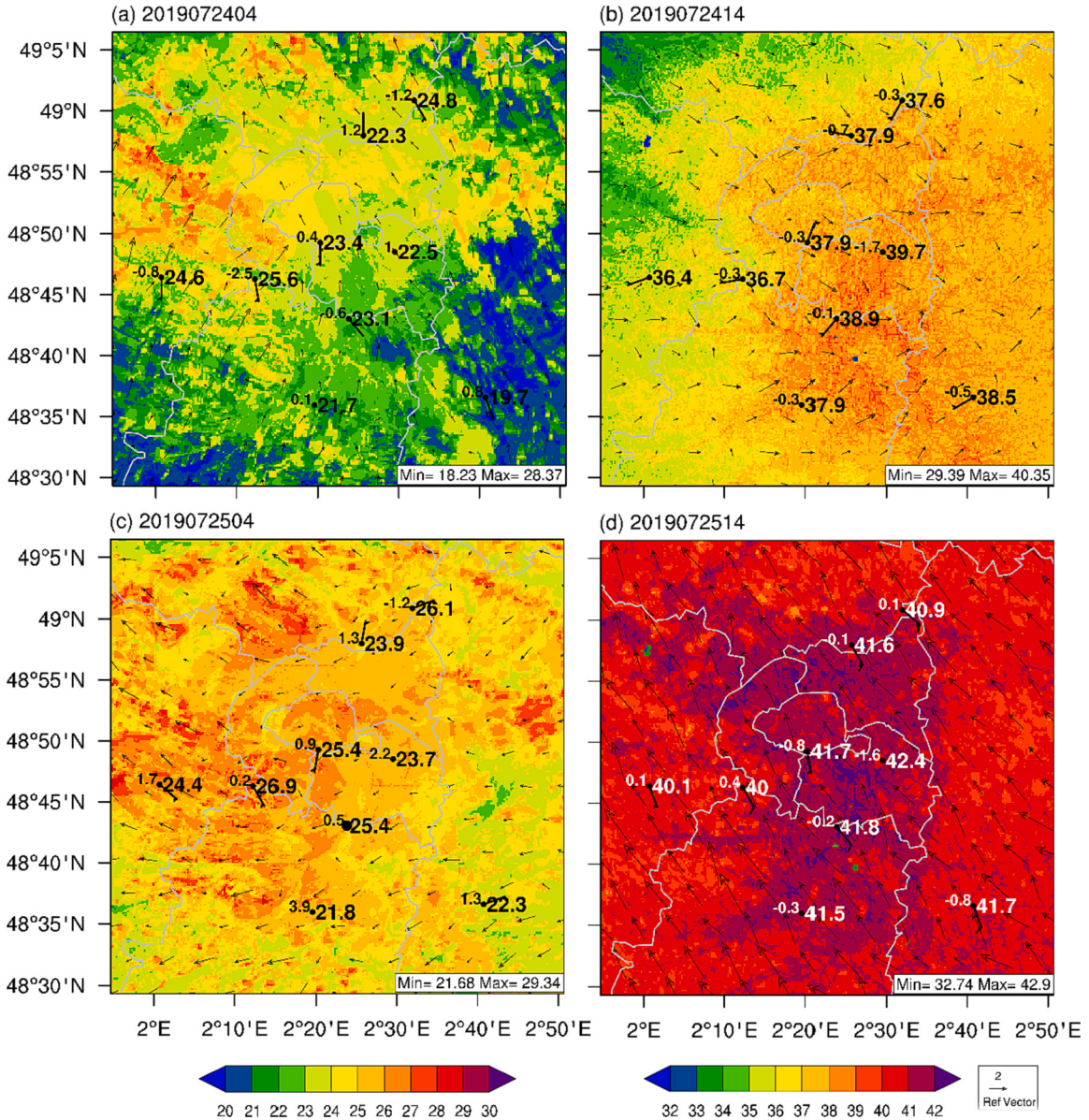


**Fig. 10.** Temperature (shaded, unit: °C) and wind field (black vectors) simulated by the d04 model (a: 04UTC on the 24th, b: 14UTC on the 24th, c: 04UTC on the 25th, d: 14UTC on the 25th) compared to observations at the station. Black dots represent observing stations, black arrows represent observed wind vectors, the values to the right of the black dots represents  $T_2_{\text{obs}}$ , and the values to the left of the black dots represent the difference between  $T_2_{\text{d04}}$  and  $T_2_{\text{obs}}$ .

the two sets of experiments at 06 and 16 local time on 24July. As was identified that, compared to NO\_URB, the URB experiment resulted in significantly higher temperatures in the city center of Paris, particularly in the morning with a temperature difference of about 8 °C (Fig. 12a). The elevated temperature areas were mainly located in the city center and the northwest downwind area. The urban underlayer reduced the near-surface wind speed in the urban area at night and caused wind speed and direction convergence within the city (Fig. 12a-b). Additionally, the urban dry island characteristics were also evident, especially during the afternoon when the urban area had the lowest relative humidity (Fig. 12c-d).

To determine the synergies between the urban thermal environment and heatwaves in Paris, the factor separation analysis (Ortiz et al., 2018) was used to extract the urban factor's contribution to local temperature under certain weather conditions. The urban factor includes the underlying urban surface and the associated physical processes, represented by the temperature difference between the URB and NO\_URB experiments. Fig. 12 shows the variation of the urban factor contribution during different stages of the heatwave event, calculated using the 111-m simulation of the central city of Paris (average of the red box in Fig. 1b) and the area-averaging method for urban grid points within the D04 region. The average value of the contribution in pre-heatwave stage was obtained

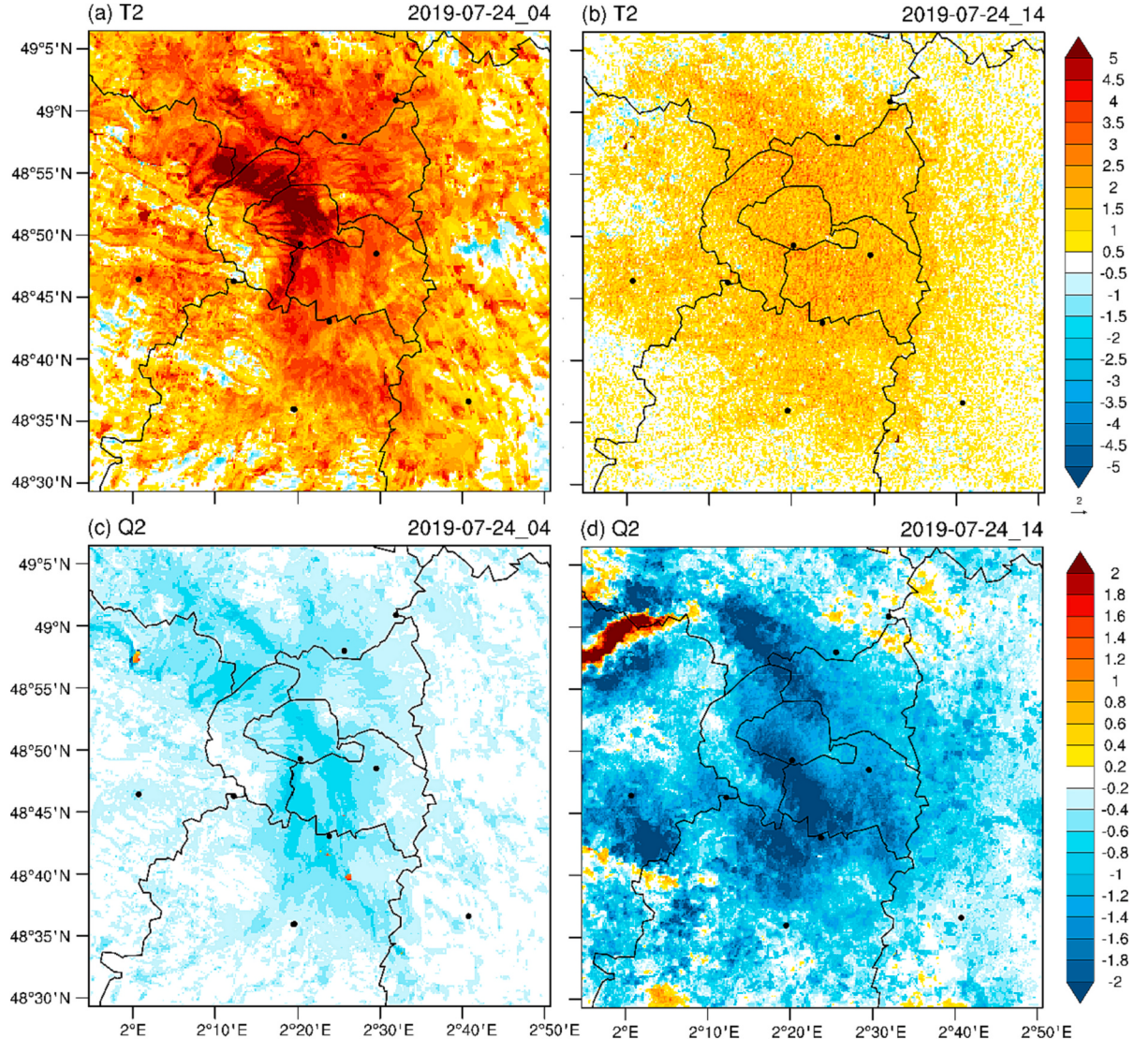


**Fig. 11.** Difference of 2-m air temperature (a-b, temperature unit: Celsius) and 2-m specific humidity (c-d, unit:  $1.0 \times 10^{-3} \text{ g} \cdot \text{kg}^{-1}$ ) between URB and NO\_URB experiments at 04UTC (a,c) and 14UTC (b, d) on July 24th.

from 19UTC to 04UTC on July 20–21 (blue shading in Fig. 12), and the average value of the contributions in the heatwave stage was obtained from 19UTC to 04UTC on July 22–25 (pink shading in Fig. 12). While the day-time mean is represented as the average during 05–18UTC 20–21July and 22–25July for the pre-heatwave and heatwave periods, respectively.

A larger temperature difference during night indicates a larger influence of urban factors under certain weather background. Before the heatwave, when cloudy conditions are preponderant, the urban factor in the central area caused a temperature increase of about 1.3 °C during the day and 1.7 °C at night. Whereas during the heatwave, with strong solar radiation and low wind speed, the urban contribution on night-time temperature increased to around 1.7 °C and 2.7 °C for day and night, with the amplifications of 0.4 °C and 1.0 °C, respectively. The temperature increase in the suburban areas was slightly lower compared to the central area, with the contribution of urban factors increasing from 1.0 °C (1.1 °C) to 1.3 °C (1.7 °C) during the heatwave when measured using the average of urban grid points within the D04 region, representing an increase of about 0.3 °C (0.6 °C) for day (night).

Table 3 represents contributions of each LCZ to temperature in different heatwave stages. The contributions to the thermal environment vary across different local climate zones, with the temperature rise of 1.1–1.6 °C during the day and 1.3–2.2 °C at night during the heatwave, in which high-rise buildings and compact buildings contribute the most to the rising temperature. It is also concluded that compared with pre-heatwave periods, the contributions to day-time temperature during heatwave periods increased by 0.3–0.4 °C, and the contributions to night-time temperature during heatwave periods increased by 0.4–1.0 °C. If not consider the relatively small building types (less than 10%), the LCZ types that contribute more to the temperature change in Paris are LCZ2, LCZ8 and LCZ9, respectively, with the contribution of about 0.3 °C to the daytime, and 0.7 °C, 0.5 °C and 0.6 °C to the night.

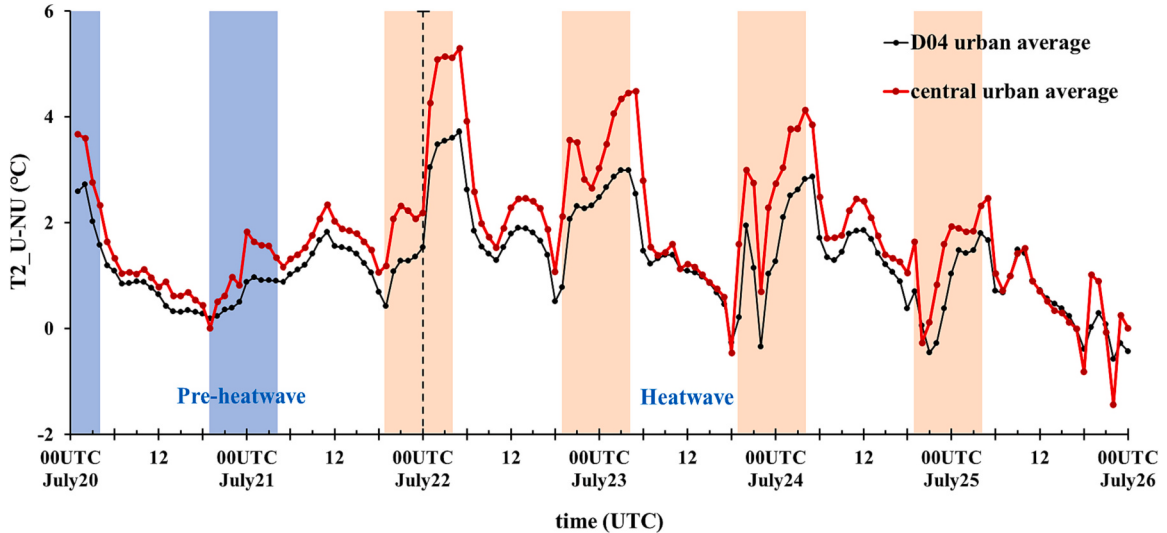


**Fig. 12.** Curves of the mean nighttime temperature difference ( $^{\circ}\text{C}$ ) over time for urban areas in tests URB and NO\_URB, where the red line is the average of the red boxed area in Fig. 1b and the black line is the average of the urban area in the D04 area, both from 111 m simulations. (For interpretation of the references to colour in this figure legend, the reader is referred to the web version of this article.)

**Table 3**

The percentage (unit: %) and individual contribution of LCZ1–10 and the regional average values of D04 and central urban area to day and night temperature in different heatwave stages, Diff is the difference between the heatwave and the pre-heatwave contribution. Units:  $^{\circ}\text{C}$ . Larger and smaller values are shaded with red and blue, respectively.

Percentage	Day-time T2(U-NU)			Night-time T2(U-NU)			
	Pre-HW	HW	DIFF	Pre-HW	HW	DIFF	
LCZ2	34.6%	1.1	1.4	0.3	1.2	2.0	0.7
LCZ3	3.7%	0.9	1.3	0.4	1.1	1.8	0.7
LCZ4	0.6%	1.2	1.6	0.4	1.2	2.2	1.0
LCZ5	5.1%	1.0	1.4	0.4	1.0	1.7	0.6
LCZ6	1.4%	0.9	1.3	0.4	1.0	1.7	0.7
LCZ8	25.5%	1.0	1.3	0.3	1.0	1.5	0.5
LCZ9	27.8%	0.8	1.2	0.4	1.0	1.5	0.6
LCZ10	1.3%	0.7	1.1	0.4	1.0	1.3	0.4
D04_avg	-	1.0	1.3	0.3	1.1	1.7	0.6
Core city	-	1.3	1.7	0.4	1.7	2.7	1.0

### 3.4. Urbanization-induced changes in the surface energy budget

To elucidate the synergistic influence mechanisms of the urbanization and the heatwave on the thermal environment in Paris, we examined the changes in the surface energy budget during the period of July 20–25 for both the URB and NO\_URB experiments (Fig. 13), all the components were averaged for the central city. Based on previous research (Ramamurthy and Bou-Zeid, 2017), the surface energy budget can be approximated as:

$$Rn + A = G + HFX + LH$$

where  $Rn$  represents the net radiation flux in the full spectrum, whose value is positive with a downward direction.  $Rn$  is further divided into net shortwave radiation ( $\text{NETSW}$ ) and net longwave radiation ( $\text{NETLW}$ ).  $A$  represents the anthropogenic heat emissions.  $HFX$  and  $LH$  represent the sensible heat flux and latent heat flux at the land surface, respectively, both of which have positive values when transported from the surface to the atmosphere.  $G$  has positive values when it is transported from the surface to the soil. The surface energy budget equation indicates that the net radiative flux received at the surface is mainly dissipated by heat transfer to the soil and the atmosphere. Considered that the anthropogenic heat is not taken into account in the BEP scheme, this paper mainly focuses

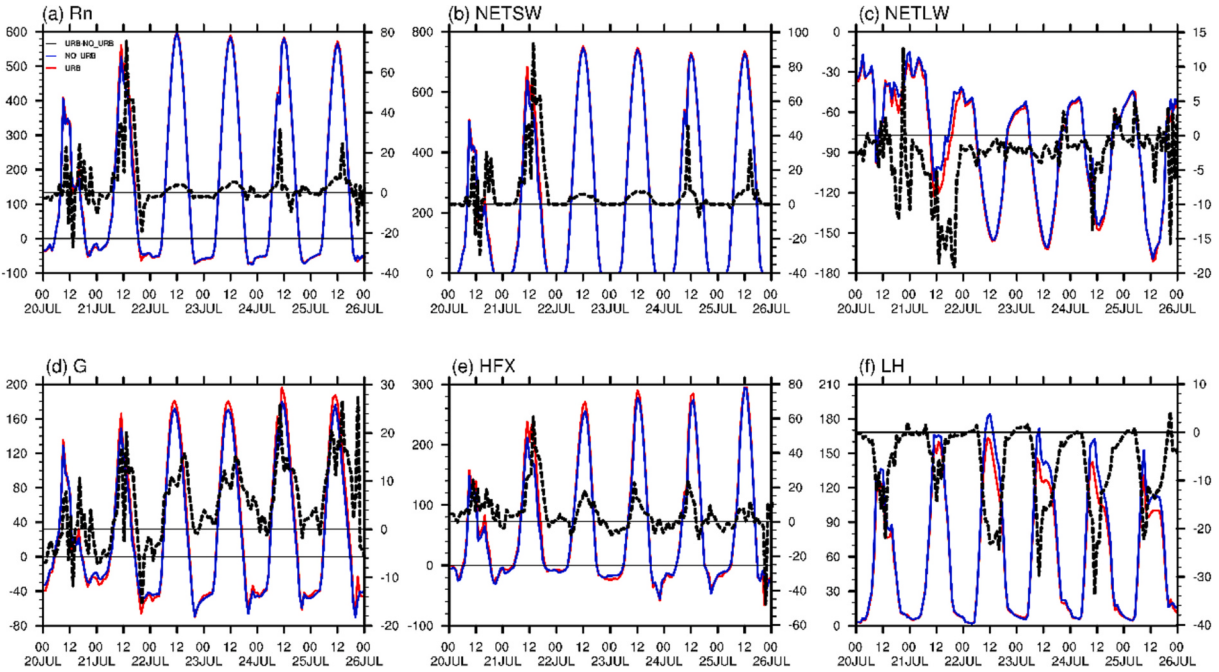


**Fig. 13.** Temporal variations of center urban averaged (red box in Fig. 1b) net radiation flux (a), incoming shortwave radiation (b), net longwave radiation (c), storage flux (d), sensible heat flux (e), and latent heat flux(f) in the URB (red) and NO\_URB (blue) experiments from July 20th to 26th, with the black line representing the difference between the red and blue lines. Units:  $\text{W/m}^2$ . The vertical axis of the black line is shown on the right side of the figure. (For interpretation of the references to colour in this figure legend, the reader is referred to the web version of this article.)

on the other four terms in the equation.

Comparing the energy budget components of the URB and NO\_URB experiments, it can be seen that the net radiation flux is slightly higher in the URB experiment, probably due to the presence of urban buildings, which increase the heating area and allow for more NETSW (Fig. 13e), resulting in a higher net radiation flux in urban areas. As is well known that impervious surfaces are mostly covered by artificial hard materials such as buildings and concrete pavements, which enhance heat absorption and release, thus increasing the surface sensible heat flux. In addition, the lack of urban vegetation cover will reduce heat transfer to the ground, contributing to the increase in lower atmospheric temperatures (Oke et al., 2017), which explains why there was higher HFX and lower LH in the URB test. Moreover, urban area has more heat storage both for the day and night in contrasted with the natural underlying. As can be concluded from the temporal variations of each energy transformation component that during the heatwave period, the  $R_n$ ,  $LH$ , and  $G$  terms all illustrated higher values during the heatwave. While the  $LH$  showed a trend of initial increase and then decrease, with the maximum value occurring in the afternoon of the 22nd. This could be attributed to the higher temperatures and lower relative humidity during the heatwave, which suppressed surface and vegetation evapotranspiration, resulting in a decrease in latent heat flux.

In conclusion, during heatwave periods in the Paris region, there is strong solar radiation and increased sensible heat flux, which directly leads to the sustained increase in near-surface air temperature during the day. In addition, urban underlying surfaces have a higher heat capacity and thermal inertia, which facilitate heat storage and cause slower daytime warming and slower nighttime cooling in urban areas. Moreover, although the urban scheme in this paper did not take into account the anthropogenic heat flux, it has already been shown in the previous studies that the higher population density and intensity of economic activities in urban areas is one of the factors contributing to the amplified urban heat island during the heatwave event.

#### 4. Summary and discussion

From July 22 to 26, 2019, Western Europe experienced an extreme heatwave. On the 25th, the temperature in Paris reached a record high of  $42.6^\circ\text{C}$ , surpassing the previous highest temperature recorded in 1947. This article used hourly situ observations, ERA5 reanalysis data and the WRF model to simulate and evaluate the extreme heatwave event. It investigated the atmospheric circulation development and the evolution mechanism of the heatwave event, analyzed the influence of urban underlayer on the local climate and its synergies with the extreme heatwave, and examined the influence of changes in the surface energy budget on the temperature during the heatwave period.

Observational and simulation results show that Paris was successively influenced by a high-pressure ridge and a pre-vortex southward flow, which provided the weather conditions for the initial large-scale subsidence motion and later enhanced warm advection during the heatwave. The high-resolution model, with a grid size of 111 m, provides more detailed horizontal and vertical gridding. By combining high-resolution land classification data and urban morphology data, it accurately represents the fine temporal

and spatial distribution characteristics of near-surface meteorological elements and reasonably simulates the intensity and diurnal variation of the Paris heat island. During the heatwave, Paris experienced strong radiative heating due to clear skies and low soil moisture, resulting in increased sensible and latent heat fluxes. Due to the higher heat storage capacity in urban, nighttime cooling in urban areas was slower, leading to a significant increase in nighttime heat island intensity during the heatwave period. Since the urban BEP scheme adopted in this paper does not consider anthropogenic heat, the influence of anthropogenic heat is not discussed in the surface energy budget analysis. Future work may consider the influence of anthropogenic heat on the urban heat island.

In this study, the factor separation method was used to eliminate the influence of urban areas on local meteorological conditions under specific weather conditions. The results showed that higher temperatures were observed in the central city and the northwestern downwind region. Prior to the heat wave, under cloudy conditions, the central area experienced a temperature increase of 1.3 °C during the day and 1.7 °C at night. However, during the heat wave, under the expected anticyclonic conditions characterized by sunny weather throughout the day and minimal wind, the temperature increased to approximately 1.7 °C during the day and 2.7 °C at night. This represented a temperature amplification of 0.4 °C and 1.0 °C, respectively, compared to the pre-heat wave conditions. Regarding the influence of the urban surface on the temperature increase, the major urban LCZ types in Paris include compact mid-rise, large low-rise, and sparsely built areas. These zones contributed 0.3 °C (0.7 °C), 0.3 °C (0.5 °C), and 0.3 °C (0.6 °C) to the daytime (nighttime) temperature change, respectively. However, this article mainly focused on the modulation effect of urban regions on local climate and the synergistic changes with an extreme heatwave in terms of near-surface meteorological elements, lacking a vertical structure analysis. It is generally believed that the influence of large-scale circulation is stronger above the boundary layer, while the influence of urban factors is bottom-up. More research and investigation are needed to understand the concrete physical processes.

#### CRediT authorship contribution statement

**Xiaojiao Ma:** Conceptualization, Methodology, Formal analysis, Investigation, Writing – original draft. **Shiguang Miao:** Conceptualization, Methodology, Supervision, Validation, Funding acquisition. **Valéry Masson:** Conceptualization, Methodology, Validation. **Jean Wurtz:** Resources, Data curation. **Yizhou Zhang:** Software, Methodology. **Jie Wang:** Software, Writing – review & editing. **Xiang-Yu Huang:** Methodology, Supervision. **Chao Yan:** Writing – review & editing.

#### Declaration of Competing Interest

The authors declare that they have no known competing financial interests or personal relationships that could have appeared to influence the work reported in this paper.

#### Data availability

The authors do not have permission to share data.

#### Acknowledgments

This study is financially supported by the National Natural Science Foundation of China (Grant 42330608), the Youth Beijing Scholars Program (Grant 2018-007), and the key innovation team of China Meteorological Administration (No. CMA2022ZD09). We would like to thank Météo-France for organizing the Olympics Games 2024 RDP and providing the in-situ observation data and urban canopy datasets.

#### References

- An, N., Dou, J., González-Cruz, J.E., Bornstein, R.D., Miao, S., Li, L., 2020. An observational case study of synergies between an intense heat wave and the urban heat island in Beijing. *J. Appl. Meteorol. Climatol.* 59 (4), 605–620. <https://doi.org/10.1175/JAMC-D-19-0125.1>.
- Anderson, G.B., Bell, M.L., 2011. Heat waves in the United States: mortality risk during heat waves and effect modification by heat wave characteristics in 43 U.S. communities. *Environ. Health Perspect.* 119, 210–218.
- Black, E., Blackburn, M., Harrison, G., Hoskins, B., Methven, J., 2004. Factors contributing to the summer 2003 European heatwave. *Weather* 59 (8), 217–223. <https://doi.org/10.1256/wea.74.04>.
- Bocher, E., Petit, G., Bernard, J., Palominos, S., 2018. A geoprocessing framework to compute urban indicators: the MapUCE tools chain. *Urban Clim.* 24, 153–174.
- Bocher, E., Bernard, J., Wiederhold, E.L.S., et al., 2021. GeoClimate: a geospatial processing toolbox for environmental and climate studies. *J. Open Source Softw.* 6 (65), 3541.
- Boutle, I.A., Finnenkoetter, A., Lock, A.P., et al., 2016. The London model: forecasting fog at 333 m resolution. *Q. J. R. Meteorol. Soc.* 142 (694), 360–371. <https://doi.org/10.1002/qj.2656>.
- Della-Marta, P.M., Haylock, M.R., Luterbacher, J., Wanner, H., 2007. Doubled length of western European summer heat waves since 1880. *J. Geophys. Res. Atmos.* 112, D15103.
- Ha, K.J., Seo, Y.W., Yeo, J.H., Timmermann, A., Chung, E.S., Franzke, C.L.E., Chan, J.C.L., Yeh, S.W., Ting, M., 2022. Dynamics and characteristics of dry and moist heatwaves over East Asia. *npj Clim. Atmos. Sci.* 5, 49.
- He, X., Wang, J., Feng, J., Yan, Z., Miao, S., Zhang, Y., Xia, J., 2020. Observational and modeling study of interactions between urban heat island and heatwave in Beijing. *J. Clean. Prod.* 247, 119169.
- He, Y., Zhu, X., Sheng, Z., He, M., 2023. Resonant waves play an important role in the increasing heat waves in northern hemisphere mid-latitudes under global warming. *Geophys. Res. Lett.* 50 <https://doi.org/10.1029/2023GL104839> e2023GL104839.
- Heaviside, C., Vardoulakis, S., Cai, X.M., 2016. Attribution of mortality to the urban heat island during heatwaves in the west midlands, UK. *Environ. Health* 15 (Suppl. 1), 27. <https://doi.org/10.1186/s12940-016-0100-9>.

- Hollósi, B., Žuvela-Aloise, M., Oswald, S., et al., 2021. Applying urban climate model in prediction mode—evaluation of MUKLIMO\_3 model performance for Austrian cities based on the summer period of 2019. *Theor. Appl. Climatol.* 144 (3), 1181–1204. <https://doi.org/10.1007/s00704-021-03580-6>.
- Laaidi, K., Zeghnoun, A., Douset, B., et al., 2012. The impact of heat islands on mortality in Paris during the August 2003 heat wave. *Environ. Health Perspect.* 120, 254–259. <https://doi.org/10.1289/ehp.1103532>.
- Lhotka, O., Kyselý, J., 2022. The 2021 European heat wave in the context of past major heat waves. *Earth Space Sci.* 9 (11) <https://doi.org/10.1029/2022EA002567>.
- Li, D., Bou-Zeid, E., 2013. Synergistic interactions between urban heat islands and heat waves: the impact in cities is larger than the sum of its parts. *J. Appl. Meteorol. Climatol.* 52, 2051–2064.
- Li, D., Sun, T., Liu, M., Yang, L., Wang, L., Gao, Z., 2015. Contrasting responses of urban and rural surface energy budgets to heat waves explain synergies between urban heat islands and heat waves. *Environ. Res. Lett.* 10, 054009.
- Li, Y.H., Miao, S.G., Chen, F., et al., 2017. Introducing and evaluating a new building-height categorization based on the fractal dimension into the coupled WRF/urban model. *Int. J. Climatol.* 37 (7), 3111–3122.
- Ma, X.J., Chen, M., Huang, X.Y., Miao, S.G., Li, Y., 2023. Hectometer scale meteorological numerical simulation: a systematic literature review and future development trends. *Chin. J. Geophys.* 66 (5), 1911–1930. <https://doi.org/10.6038/cjg2022Q0216> (in Chinese).
- Miao, S.G., Chen, F., 2014. Enhanced modeling of latent heat flux from urban surfaces in the Noah/single-layer urban canopy coupled model. *Sci. China Earth Sci.* 57 (10), 2408–2416.
- Miao, S.G., Chen, F., LeMone, M.A., et al., 2009. An observational and modeling study of characteristics of urban heat island and boundary layer structures in Beijing. *J. Appl. Meteorol. Climatol.* 48 (3), 484–501. <https://doi.org/10.1175/2008JAMC1909.1>.
- Oke, T.R., Mills, G., Christen, A., Voogt, J.A., 2017. *Urban Climates*. Cambridge University Press, Cambridge. <https://doi.org/10.1017/9781139016476>.
- Ortiz, L.E., Gonzalez, J.E., Wu, W., Schoonen, M., Tongue, J., Bornstein, R., 2018. New York City impacts on a regional heat wave. *J. Appl. Meteorol. Climatol.* 57 (4), 837–851.
- Park, K., Jin, H.G., Baik, J.J., 2023. Contrasting interactions between urban heat islands and heat waves in Seoul, South Korea, and their associations with synoptic patterns. *Urban Clim.* 49 (August 2022), 101524. <https://doi.org/10.1016/j.uclim.2023.101524>.
- Ramamurthy, P., Bou-Zeid, E., 2017. Heatwaves and urban heat islands: a comparative analysis of multiple cities. *J. Geophys. Res. Atmos.* 122, 168–178.
- Ramamurthy, P., González, J., Ortiz, L., Arend, M., Moshary, F., 2017. Impact of heatwave on a megacity: an observational analysis of New York City during July 2016. *Environ. Res. Lett.* 12, 054011.
- Richard, Y., Pohl, B., Rega, M., Pergaud, J., Thevenin, T., Emery, J., Dudek, J., Vairet, T., Zito, S., Chateau-Smith, C., 2021. Is urban heat island intensity higher during hot spells and heat waves (Dijon, France, 2014–2019)? *Urban Clim.* 35, 100747.
- Ronda, R.J., Steeneveld, G.J., Heusinkveld, B.G., et al., 2017. Urban finescale forecasting reveals weather conditions with unprecedented detail. *Bull. Am. Meteorol. Soc.* 98 (12), 2675–2688. <https://doi.org/10.1175/BAMS-D-16-0297.1>.
- Rousi, E., Kornhuber, K., Beobide-Arsuaga, G., Luo, F., Coumou, D., 2022. Accelerated western European heatwave trends linked to more-persistent double jets over Eurasia. *Nat. Commun.* 13 (1), 1–11. <https://doi.org/10.1038/s41467-022-31432-y>.
- Salamanca, F., Krpo, A., Martilli, A., et al., 2010. A new building energy model coupled with an urban canopy parameterization for urban climate simulations—part I. Formulation, verification, and sensitivity analysis of the model. *Theor. Appl. Climatol.* 99 (3–4), 331–344. <https://doi.org/10.1007/s00704-009-0142-9>.
- Stefanon, M., Dandrea, F., Drobinski, P., 2012. Heatwave classification over Europe and the Mediterranean region. *Environ. Res. Lett.* 7 (1) <https://doi.org/10.1088/1748-9326/7/1/014023>.
- Stott, P.A., Christidis, N., Otto, F.E., Sun, Y., Vanderlinden, J.P., van Oldenborgh, G.J., Vautard, R., von Storch, H., Walton, P., Yiou, P., Zwiers, F.W., 2016. Attribution of extreme weather and climate-related events. *Wiley Interdiscip. Rev. Clim. Chang.* 7 (1), 23–41. <https://doi.org/10.1002/wcc.380>.
- Tan, J., Zheng, Y., Song, G., Kalkstein, L.S., Kalkstein, A.J., Tang, X., 2007. Heat wave impacts on mortality in Shanghai, 1998 and 2003. *Int. J. Biometeorol.* 51, 193–200.
- Taylor, K.E., 2001. Summarizing multiple aspects of model performance in a single diagram. *JGR* 106 (D7), 7183–7192. April 16, 2001.
- Yang, J.B., Liu, H.N., Sun, J.N., et al., 2015. Further development of the regional boundary layer model to study the impacts of greenery on the urban thermal environment. *J. Appl. Meteorol. Climatol.* 54 (1), 137–152.
- Zhang, Y.Z., Miao, S.G., Dai, Y.J., et al., 2013. Numerical simulation of characteristics of summer clear day boundary layer in Beijing and the impact of urban underlying surface on seabreeze. *Chin. J. Geophys.* 56 (8), 2558–2573. <https://doi.org/10.6038/cjg20130806>.
- Zhao, L., Oppenheimer, M., Zhu, Q., Baldwin, J.W., Ebi, K.L., Bou-Zeid, E., Guan, K., Liu, X., 2018. Interactions between urban heat islands and heat waves. *Environ. Res. Lett.* 13 (3) <https://doi.org/10.1088/1748-9326/aa9f73>.
- Zhou, B.W., Li, Y.H., Miao, S.G., 2021. A scale-adaptive turbulence model for the dry convective boundary layer. *J. Atmos. Sci.* 78 (5), 1715–1733. <https://doi.org/10.1175/jas-d-20-0240.1>.